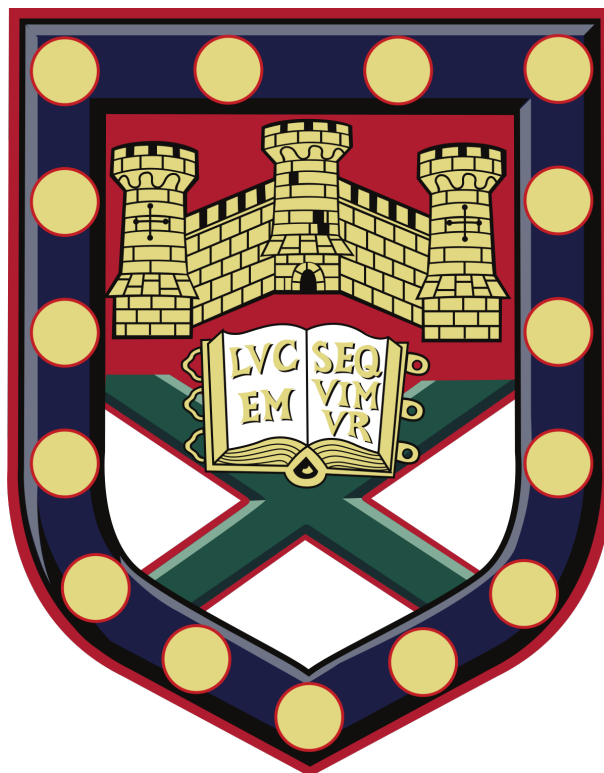


Developing an Original N-Body Code for Use in Modelling the Arp 240 (NGC 5257/58) Galactic Interaction

Jeremy Godden

Supervisors:
Professor Clare L. Dobbs,
Dr Steven Rieder.



College of Engineering, Mathematics and Physical Sciences
University of Exeter
27th April 2020

Abstract

The aim of this investigation was to create an N-Body program capable of simulating galactic interactions and demonstrate its competency through modelling a novel, observed interaction. An N-Body code was developed, making use of an octree function to reduce computational complexity, capable of simulating basic galaxies during interactions. The program has a substantial run time for large N simulations, partially due to the chosen programming language, limiting the feasible size of conducted simulations. Observational data and simplified, time-reversed simulations were used to determine initial conditions of the Arp 240 galaxy system, which exhibits visually clear interaction features. The precision of the initial conditions diminished due to the high volume of time-reversed simulations required, of which a fraction were able to be completed. Preliminary results display general similarities to the system's morphological features, recreating the observed tidal bridge, tails and spiral structures, but it's orbit deviates from predictions. However, an improperly calibrated model of dynamical friction used in the simulations rendered these results, and derived initial conditions, unreliable. Limited use of live dark matter halos produce an orbit expected of the Arp 240 galaxies. It is concluded that the program is not currently suitable to accurately simulate detailed galactic interactions, but with further work could become a useful tool to do so.

Contents

1	Introduction	4
1.1	Aims	5
2	Background Theory	6
2.1	Galaxy Structure	6
2.2	Galactic Interactions	7
2.3	N-Body Codes	10
3	Arp 240	11
3.1	Observational Evidence for an Interaction	11
3.2	Deriving Current Information	12
4	The N-Body Program	13
4.1	Modelling the Galaxies	13
4.2	Notable Code	15
4.3	Validation Checks	18
4.4	Program Limitations	18
5	Method	19
5.1	Finding Initial Conditions	19
5.2	Simulating the Interaction	20
6	Results & Analysis	21
6.1	Determining Initial Conditions	21
6.2	Preliminary Simulation	22
6.3	Live Dark Matter Halo Simulations	28
7	Discussion	30
7.1	Technical Limitations	30
7.2	Initial Conditions	30
7.3	Preliminary Simulation	30
7.4	Live Dark Matter Halo Simulations	31
7.5	Program Performance	31
8	Conclusion	32
8.1	Future Work	32
Acknowledgements		34

CONTENTS

Appendix A Galactocentric Rest Frame	35
Appendix B Accessing Written Code	36
Appendix C Downloading and Operating HaloGen	37
Appendix D Galactic Modelling Parameters	38
Appendix E Retrograde Passages	39
Appendix F Post Second Close Encounter Morphology	40
Bibliography	42

1. Introduction

Morphological features, such as spiral arms, bridges and tails, are some of the most striking properties observed in galaxies, conveying crucial information about their history. These characteristics imply that a galaxy has undergone a close encounter with another, altering its fundamental structures. Spiral arms specifically are an important consequence of these interactions as they are areas of high baryonic density with increased star formation [1], that play a major role in the secular evolution of their host galaxies [2]. Spiral arms are seen in nearly two thirds of all observed galaxies [3], thus it is important to explore how they, along with other morphological features, form during interactions.

Numerical simulations play a vital role in theoretical studies on cosmological structure formation, providing the most accurate predictions on cosmological processes due to their intrinsically large observational time scales. Building upon available resources in this field allows for more investigations to be undertaken with greater ease.

Instrumental work was done in Toomre & Toomre, 1972 [4], to first produce simple computational models of galactic interactions. Whilst these simulations were basic, using simplifications and now outdated models, they clearly displayed tidal features, analogous to those identified in observed interactions.

Due to the increase in technical capabilities, both hardware and the computational efficiency of N-Body programs, the research into galactic interactions has rapidly developed and become significantly more advanced. One of many comprehensive N-Body Codes is GADGET-2, whose methods and algorithms are outlined in Springel, 2005 [5].

Multiple previous investigations have modelled systems of interacting galaxies using advanced numerical simulations. Such systems include: M51 (modelled by both Salo & Laurikainen, 2000 [6], and Dobbs *et al.*, 2010 [7]), the NGC1512/1510 pair (seen in Koribalski *et al.*, 2009 [8]), and NGC 6872 (as modelled in Horellou & Koribalski, 2007 [9]).

Specifically, the work done by Semczuk *et al.*, 2018 [10], to model the interaction between the M31 and M33 galaxies, inspired this investigation. During that study a detailed simulation was conducted, using GADGET-2, to allow for the morphologies of each galactic component to be accurately observed during the interaction.

Numerous investigations have been carried out on the different types of spiral arms and their origins, as well as the consequences they have for their host galaxy. Dobbs & Baba, 2014 [11],

conducted a concise review on all spiral arm classifications, including those formed by galactic interactions.

1.1 Aims

The purpose of this investigation is to develop a basic, computationally efficient N-Body code, capable of simulating galaxy interactions. The program will subsequently be used to recreate observed tidal features of a known, novel system of interacting galaxies. If accurately done, the entire interaction will be simulated, to determine the history, futures and the ensuing structures of the galaxies involved.

2. Background Theory

2.1 Galaxy Structure

A galaxy is a gravitationally bound system of stars, dust, gas and dark matter [12]. Its components can be seen in Figure 2.1. Baryonic matter, consisting of gas, dust and stellar masses, can be found in the bulge and the disk of the galaxy. Dark matter, whose mass usually dominates over baryonic matter's, is thought to be found in a halo that encompasses the other galactic components. A dark matter halo (DMH) is hypothesized from the theory of cold dark matter (CDM), where dark matter weakly interacts with ordinary matter, and moves slowly compared to the speed of light [13].

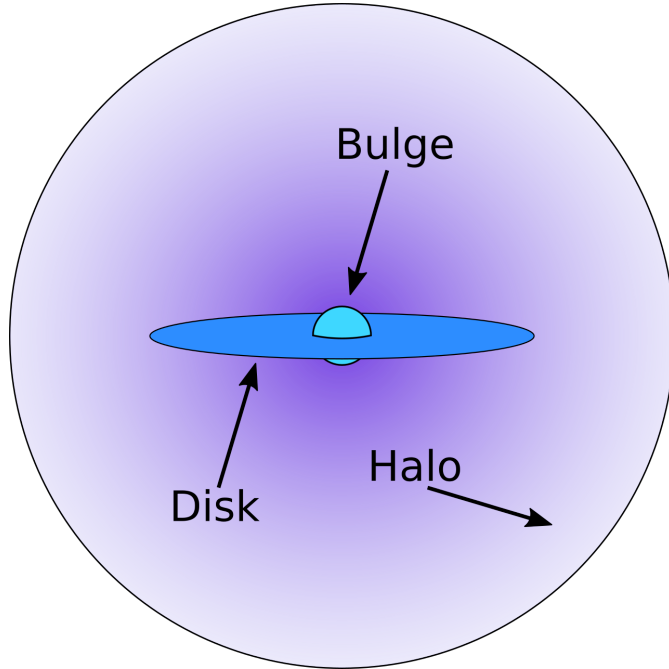


Figure 2.1: A graphic displaying components of a galaxy.

Galaxies were first classified, in a basic manner, by their structure in 1926 by Edwin Hubble [14]. They fall into three main categories: elliptical, spiral and lenticular, all of which are displayed in Figure 2.2. Whilst outdated, this classification is suitable for the needs of this study.

Elliptical galaxies are elliptically shaped on the sky and featureless, with a light distribution that fades smoothly from a bright centre [14]. Spiral galaxies have a flat disk with areas of high density, known as spiral arms. They also have a central bulge that resembles an elliptical galaxy, as well as possibly having a central bar to which the spiral arms connect. Lenticular galaxies are similar to spiral galaxies; however, they contain a featureless flat disk, devoid of spiral arms and possess a smooth light distribution. They contain little or no interstellar gas or dust [15], leading to very little star formation. On top of these categories there are irregular galaxies, which have no defined shape and are inconsistent from one to another.

It is estimated that about 15% of all observable galaxies are elliptical, roughly 60% are thought to be spiral galaxies and $\sim 20\%$ lenticular [16].

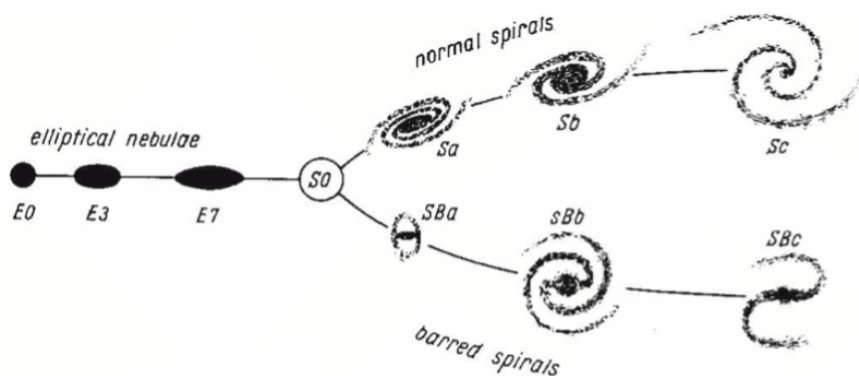


Figure 2.2: A display of Hubble's "Tuning Fork" sequence for galaxy classification [17].

There are three categories of spiral arms in spiral galaxies: grand-design, multi-armed and flocculent. Grand-design spiral galaxies tend to have two large, symmetric arms, of high-density matter, in their disks and are present in 60% of all disk galaxies [11]. They are theorised to be primarily induced by tidal interactions, the presence of a central bar, or obey the steady-state density wave theory (See Lin & Shu, 1966 [18]) [11]. Flocculent and multi-armed spiral galaxies have numerous less-defined arms within their disks and though flocculent arms tend to be shorter, both are thought to be produced from gravitational instabilities (See Toomre, 1964 [19]) [11]. All types of spiral arms can exhibit bars [11].

2.2 Galactic Interactions

Interactions occur when gravitational forces between two galaxies are substantial enough to influence the motion and structure of each other. Large tidal forces arise when the galaxies pass close together and are strong enough to strip the galaxies of matter and cause perturbations in their baryonic disk. These density fluctuations in the disk are known as morphological features and are best classified visually [20].

Morphological features are not the only way of determining if two galaxies have undergone, or are undergoing, an interaction. Recent and large increases in the young stellar population throughout a galaxy's disk indicates previous high star formation rates, which can be attributed to a close encounter. On top of this, mapping of H_I (neutral atomic hydrogen) regions from their emissions, seen through radio-telescopes, can be used to detect streams of gas between two galaxies that are not observable by the eye. All these reasons indicate that M33 and M31 had once had a close encounter, as explained by Semczuk *et al.*, 2018 [10].

2.2.1 Morphological Features

Tidal Tails

A tidal tail is a long, curving, uniform and faintly luminous structure that consists of baryonic matter stripped from a galaxy during an interaction [4] [21]. This matter will become isolated from the rest of the galaxy, eventually becoming uninfluenced by its gravitational forces. An example of a tidal tail can be seen in Figure 2.3.

Counterarms

A counter arm is similar to a tidal tail, however matter within a counterarm will eventually be returned to its host galaxy due to the gravitational forces [4]. As a result of this, counterarms are seen to extend to a much smaller distance than tails.

Tidal Bridges

Tidal bridges are structures of baryonic matter connecting two galaxies which are undergoing, or have undergone, an interaction [22]. Tidal bridges are not permanent and will disperse over time, similar to tidal tails. An example of a bridge can be seen in Figure 2.3.

Spiral Arms

Tidal forces, due to interactions, alter the angular momentum of matter in the disk, causing areas of high density to form. These areas compact dust and gas, which in turn will form stars, making spiral arms areas of high star formation rates [23]. Due to this increase of stars, the arms become more luminous, making them easier to see in visible light. An example of spiral arms can be seen in Figure 2.4.

Bars

Bars are elongated structures of baryonic matter that extend outwards from opposite sides of the galactic centre. They are found in roughly one third of all disk galaxies and are formed

by inherent galactic processes or interactions [24]. They are often associated with spiral arms, which can appear to begin at the edge of the bar. An example of a bar can be seen in Figure 2.4.

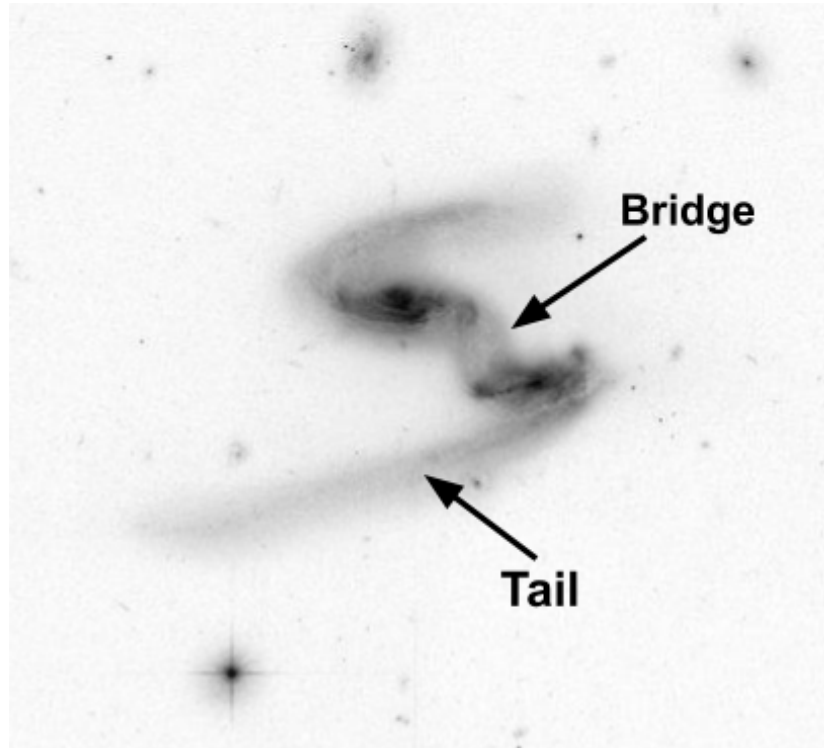


Figure 2.3: An observational image of the ESO 77-14 system of galaxies [25], in negative colour to more clearly see morphological features present. It is labelled to indicate the tidal bridge and tail present.

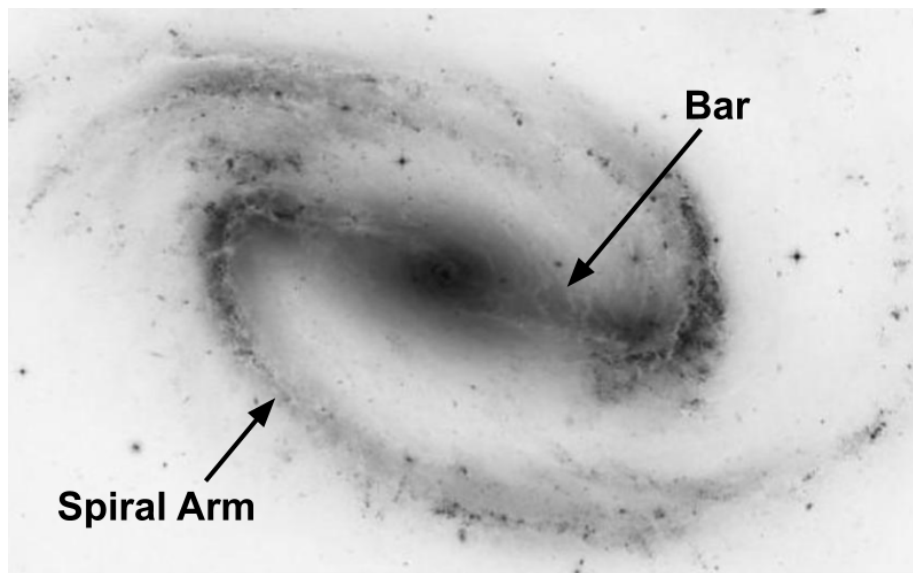


Figure 2.4: An observational image of the NGC 1300 galaxy [26], in negative colour to more clearly see morphological features present. It is labelled to indicate the spiral arms and bar present.

2.2.2 Prograde and Retrograde Passages

A galaxy has a prograde passage if its disk matter is orbiting its centre in the same direction as the galaxy is moving. Thus, a retrograde passage occurs when a galaxy's disk matter is orbiting the centre in the opposite direction to it's motion. A galaxy with a prograde passage during an interaction will be more tidally violent, creating strong morphological features and disk perturbations [4]. In contrast, retrograde passages are less tidally violent during interactions, producing softer morphological features [4].

2.2.3 Interaction Conclusion

Close encounters of galaxies can conclude in one of two ways. The system can have a parabolic passage where they will briefly orbit each other before separating and becoming gravitationally unbound. These interactions tend to be much milder. Alternatively, the interaction can result in a merger, where the two galaxies closely orbit one another for a time before eventually combining into a larger galaxy. Interactions that end in mergers are often more violent, ejecting large amounts of matter [4].

2.3 N-Body Codes

An N-Body simulation is a collection of N particles mapped on a set space, all under the influence of a set of physical forces. The motion of each body is found by solving a set of ordinary differential equations that correspond to the forces acting upon the body.

The first instance of an N-Body simulation used for galactic interactions was engineered by Holmberg, 1941 [27], where stars were modelled as light bulbs, with the mathematical equivalence of light propagation and gravitational force being used to predict their movement. Even in this primitive method, spiral arms were able to be seen in a basic galaxy interaction.

Since then, continuous progress has been made to increase the accuracy and speed of modelling large systems in N-Body codes, due to the production of more efficient hardware and the creation of algorithms to decrease the computational complexity of the code. Examples of such algorithms are the Barnes-Hut tree algorithm [28], which approximates distant bodies as one if they are far enough away from the body in question, and the Fast Multipole Method [29], which allows the grouping of nearby bodies to be treated as one. These advancements have resulted in the numerous advanced, open source N-Body codes available today, such as NEMO [30] and, more recently, GADGET-2 [5].

3. Arp 240

3.1 Observational Evidence for an Interaction

Figure 3.1 shows an observation of the Arp 240 system, which will be the subject of investigation within this study. The Arp 240 system contains two galaxies of roughly equal mass [31], named NGC 5257 and NGC 5258. From inspection alone it can be inferred that these two galaxies are interacting, due to the prominence of their morphological features in visible light. These take the form of a faint bridge between the two, supposed tidal tails and clear spiral structures in both disks.



Figure 3.1: Top: Observation [32] of the Arp 240 system of galaxies. Left is NGC 5257, right is NGC 5258. Bottom: Negative colour observation to allow for morphological features to be more easily discerned.

Iono *et al.*, 2005 [33], used H_I observations to map atomic gas within the system, providing

further evidence that an interaction is occurring. It is also inferred that the system will result in a merger [33]. Privon *et al.*, 2013 [34], deduced from this that the system has a weak tidal coupling, of which most of the disturbance is along the line of sight. It is also hypothesized that the interaction is prograde in order to reproduce the tidal tail seen in NGC 5258 [34].

Privon *et al.*, 2013 [34], conducted a set of simple simulations to model a set of interacting galaxies, including Arp 240, using Identikit, outlined by Barnes & Hibbard, 2009 [35]. Identikit is a program capable of producing basic simulations of interacting galaxies, through the use of massless test-particles in the galaxies' disks. In addition, Holincheck *et al.*, 2016 [36], conducted an investigation where Identikit was again used to generate numerous simulations of random galactic interactions. These were matched to observed interactions, one of which being Arp 240, via visual resemblance done by public volunteers, allowing for the simulation to be further investigated.

Whilst there have been previous dynamical models of Arp 240, none have been conducted in as much detail as intended in this study. This is one of the principal reasons it was chosen to be investigated.

Observational data for this system is taken from a recent study by Fuentes-Carrera *et al.*, 2019 [31], which contains necessary information to model the galaxies.

3.2 Deriving Current Information

The distance to each galaxy, and their positions on the sky [31], can be used to find the positions of each galaxy in 3D space, then being converted to galactocentric rest frame coordinates (see Appendix A). Subsequent placing of NGC 5258 at the origin results in NGC 5257 having a position vector equivalent to the relative distance between the galaxies. This gives the current, relative position coordinates seen in Table 3.1.

Additionally, the normalised spin of both galaxies' disks can be derived from observational data [31], allowing for their correct orientation. The normalised spin of a galactic disk is the normalised vector that points perpendicular to the plane of the disk. These values for both disks can be seen in Table 3.1.

Vector	X	Y	Z	Units
Relative Position	-211.9	547.5	129.5	<i>kpc</i>
Normalised Spin of NGC 5257	0.992	0.118	0.048	-
Normalised Spin of NGC 5258	0.547	-0.800	-0.246	-

Table 3.1: Current relative positions of Arp 240 system and their normalised disk spins.

Due to the galaxies being at such a large distance away, their proper motion cannot be observed and thus their velocities are unknown. This is overcome by using an orbit integration scheme to find initial conditions (See Section 5.1).

4. The N-Body Program

The N-Body code and analysis functions developed during this study are written in the Python programming language, chosen as it is well suited for novice programmers. Information on accessing the code can be found in Appendix B.

4.1 Modelling the Galaxies

4.1.1 Baryonic Matter

For simplicity, the bulge of the galaxy is modelled as a single massive particle at the centre. It contains all of the baryonic mass expected in the bulge.

The baryonic disk is modelled as a lenticular disk of particles. The total baryonic mass of a galaxy's disk is equally allocated among all particles modelling it. A normal distribution, as seen in Equation 4.1, is used to generate an orbital radius about the galactic centre for each particle in the disk, between $(0.05 - 1)R_d$, where R_d is the galaxy's maximum disk radius.

$$f = \frac{1}{\sigma \sqrt{2\pi}} \exp\left(-\frac{1}{2} \left(\frac{x - \mu}{\sigma}\right)^2\right). \quad (4.1)$$

μ and σ are varied in order to fit the expected mass distribution of the galaxy disk being modelled. Disk particles are not given a radius within $0.05 R_d$ to allow for a separation between the modelled disk and bulge. It is important to use a large number of particles, $N > 500$, within a disk of this nature, to avoid a mass imbalance. Having a small N can result in the simulation concentrating mass on one side of the disk, leading to inaccurate results.

For preliminary simulations, the disk particles have the option to be made massless to reduce the computational complexity of the code. Massless particles do not exert gravitational forces on other particles but are still perturbed by forces from massive particles. When using this simplification, the mass of the baryonic matter in the disk is added to the mass of the central bulge particle.

4.1.2 Dark Matter

The dark matter in each galaxy is modelled using an NFW (Navarro-Frenk-White) profile [37], which shows the density of the DMH at radius r :

$$\rho(r) = \frac{\rho_0}{\frac{r}{R_s} \left(1 + \frac{r}{R_s}\right)^2}, \quad (4.2)$$

where ρ_0 is the critical density of the DMH and R_s is its scale radius. These are galactic parameters specific to each galaxy.

This profile is chosen as it is commonly used when modelling DMHs, making it straightforward to replicate and produce using pre-existing programs.

Live Dark Matter Halo

HaloGen, a program within AMUSE (Astrophysical Multipurpose Software Environment) [38] [39] [40] [41], is used to create a live DMH of massive particles (See Appendix C for guidelines on accessing and operating AMUSE/HaloGen). They are distributed according to the NFW profile.

Potential Dark Matter Halo

A potential DMH is the gravitational potential of the halo profile, coupled with dynamical friction.

The gravitational potential of the NFW profile is found by solving Poisson's equation, resulting in:

$$\psi(r) = -\frac{4\pi G \rho_0 R_s^3}{r} \ln\left(1 + \frac{r}{R_s}\right). \quad (4.3)$$

This is then used to find the acceleration due to the halo:

$$\mathbf{a} = -\frac{d\psi_{NFW}(r)}{dr} = \frac{GM_{vir}}{\ln(1+c) - \frac{c}{(1+c)}} \frac{\frac{r}{(r+R_s)} - \ln\left(1 + \frac{r}{R_s}\right)}{r^3} \vec{r}, \quad (4.4)$$

where c is the concentration parameter, which is unique to each halo, and M_{vir} is the mass of the DMH.

This must be paired with an equation for dynamical friction in order to accurately recreate the DMH without live particles. Dynamical friction is the drag force a large body feels as it moves through a field of massive particles. Momentum is transferred from the large mass to the smaller ones, slowing the former.

The equation for acceleration due to dynamical friction used is the Chandrasekhar formula [42]:

$$\mathbf{f}_{DF} = -\frac{4\pi G^2 M \ln \Lambda \rho(r)}{v^2} \left(\text{erf}(X) - \frac{2X}{\sqrt{\pi}} \exp(-X^2) \right) \frac{\vec{v}}{v}, \quad (4.5)$$

where M is the mass of the body passing through the halo, and $\rho(r)$ is the density distribution of the halo. For the coulomb logarithm ($\ln \Lambda$), the formula from Hashimoto *et al.*, 2003 [43], was used:

$$\ln \Lambda = \ln \left(\frac{r}{1.4\epsilon} \right), \quad (4.6)$$

where ϵ is the softening length of the galaxy subject to dynamical friction. Within Equation 4.5, $X = v/\sqrt{2}\sigma$, where σ is the 1D velocity dispersion, found using [44]:

$$\sigma \approx V_{max} \frac{1.4393x^{0.354}}{1 + 1.1756x^{0.725}}, \quad (4.7)$$

with V_{max} being the maximum circular velocity of disk matter.

Using a DMH potential greatly decreases the run time of the simulation due to there being far fewer particles within the simulation. However, it does not take into account the tidal stripping of the DMH.

4.2 Notable Code

The code written during this investigation uses a velocity Verlet, leapfrog integration system [45] to progress the simulation forwards in time:

$$\begin{aligned} v_{i+\frac{1}{2}} &= v_i + a_i \frac{dt}{2}, \\ \text{with } a_i &= \frac{F(x_i)}{m}, \\ x_{i+1} &= x_i + v_{i+\frac{1}{2}} dt, \\ v_{i+1} &= v_{i+\frac{1}{2}} + a_i \frac{dt}{2}. \end{aligned} \quad (4.8)$$

A leapfrog integration system is used as it accurately conserves energy between steps. A velocity Verlet integration system is chosen as it is time reversible, which is required to find the initial conditions of the galaxies (see Section 5.1).

A Barnes-Hut tree algorithm [28] is used to decrease the computational complexity of the simulation. A tree algorithm functions by recursively splitting each section of the 3D simulation space into 8 smaller, equal nodes, until each node contains either 1 or 0 bodies, creating an octree. A 2D example is seen in Figure 4.1.

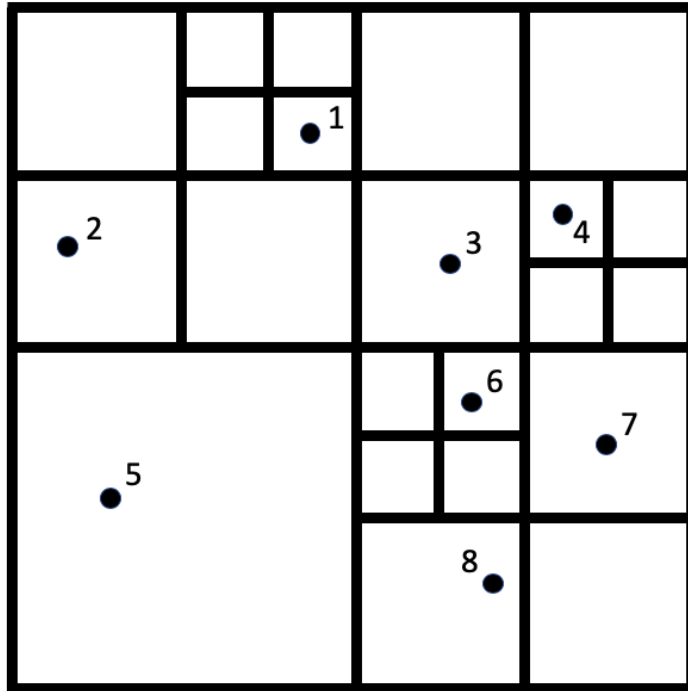


Figure 4.1: An example of a 2D space being split up, using a tree code. Due to it being a 2D space, each section is only split up into 4 smaller sections.

To calculate the force on a particle p , the octree is traversed from root (the original node) to leaf (the smallest node that contains a single body), calculating the quotient:

$$\theta = \frac{s}{d}, \quad (4.9)$$

where s is the width of the current node and d is the distance between particle p and the current node's centre of mass. This quotient is used to decide whether the group of bodies in a node are sufficiently far away from p to be approximated as one. If θ is below a threshold value, chosen to be 0.5 in this study from data shown in Figure 4.2, then the group of bodies can be approximated. This reduces the number of force calculations from $O(N^2)$ to $O(N \log(N))$.

Figure 4.3 shows how the Barnes-Hut algorithm compares to regular force calculations. At low values of N , regular force calculations are more efficient. When the number of particles rises above 100, the Barnes-Hut method becomes more effective.

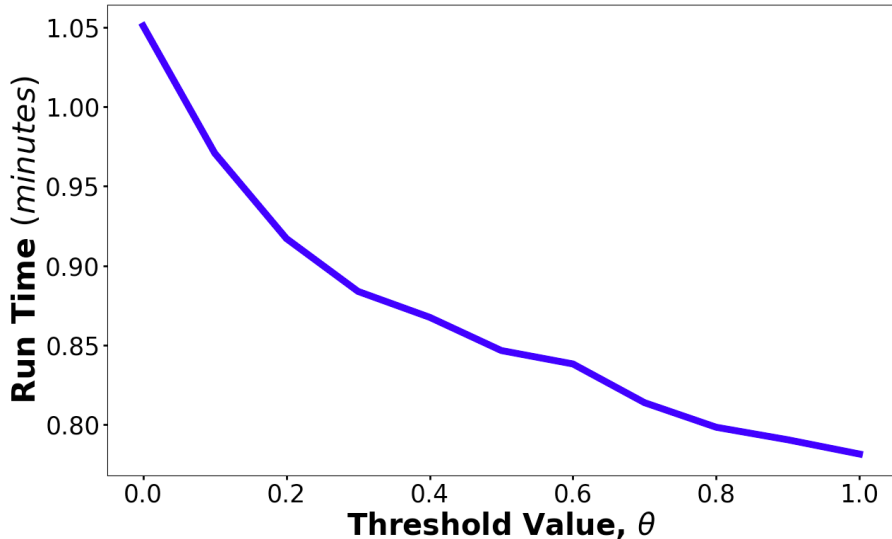


Figure 4.2: Comparing the run time of identical trial simulations with various threshold values, θ . Credit: Amy Hewitt.

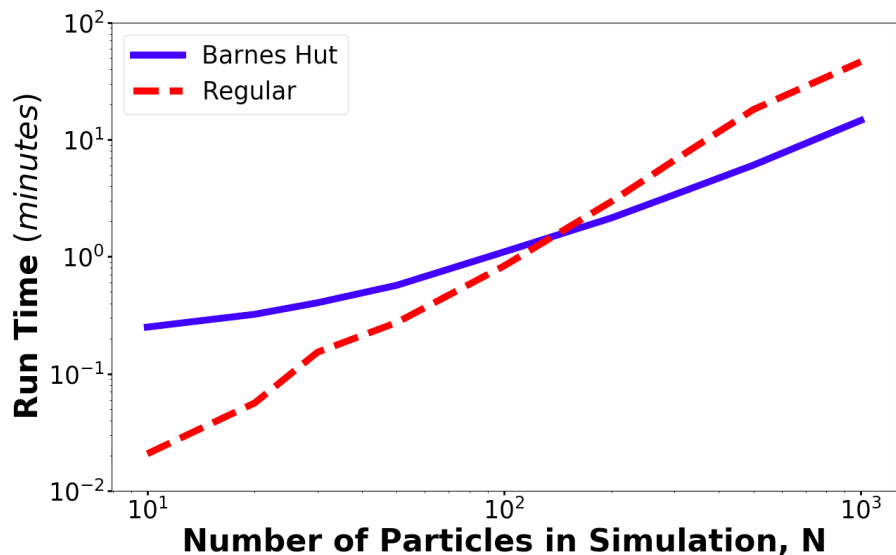


Figure 4.3: Comparison of the Barnes-Hut algorithm with regular force calculations using simple, identical simulations with a varying total number of particles, N . Credit: Amy Hewitt.

In addition to this, a softening parameter was implemented so that the interactions are modelled as collisionless systems. A softening parameter is included in Newton's law of gravitation, seen in Equation 4.10, to prevent the gravitational forces from rapidly increasing to enormous values between two very near bodies, due to the r^{-2} dependence. Without one, singularities will occur, where particles suddenly and quickly separate from a system after passing close to one another, dramatically increasing their acceleration.

$$F = -\frac{Gm_1m_2}{r^2 + \epsilon_{soft}^2}. \quad (4.10)$$

The softening parameter used, ϵ_{soft} , took the form of:

$$\epsilon_{soft} = 0.98N^{-0.26}, \quad (4.11)$$

as recommended by Athanassoula *et al.*, 2000 [46], for systems with $30 < N < 300000$.

4.3 Validation Checks

The total kinetic and potential energies can be found at each time step during a simulation, and plotted afterwards, in order to confirm that the energy is conserved throughout the interaction. This is key to ensuring the accuracy of the simulation. Cumulative error is a way of quantifying the total energy variations during a simulation and is calculated using the formula:

$$E_{cumu} = \sum \frac{|PE_i - PE_{i-1} + KE_i - KE_{i-1}|}{E_0}, \quad \text{with } E_0 = |PE_0| + |KE_0|. \quad (4.12)$$

The smaller E_{cumu} is, the more accurate the simulation.

3D plotting functions can also be used to visually observe the simulated interaction and confirm that it developed as expected. In addition, a simulated galaxy's rotation curve can be plotted, allowing for comparisons to observational data.

4.4 Program Limitations

Overall, the simulations used in this investigation are basic. They do not separate baryonic mass into sets of matter (e.g. gas, dust and stellar population), instead modelling them all together. Furthermore, the bulge is not modelled using a mass distribution, but a single particle. Although both of these choices result in an inability to accurately recreate exact morphologies in each galactic component, the code is still able to demonstrate general morphologies.

In addition, galaxy components in the simulations are not created in conjunction with each other. An example is that the live halo and baryonic disk are made separately, which leads to instabilities in the model when combining them. Work is done to diminish these inaccuracies by adjusting the velocity of the disk particles to ensure that the virial theorem, shown in Equation 4.13, is met at the time of combination.

$$E_{totalkinetic} = -\frac{1}{2}E_{totalpotential}. \quad (4.13)$$

5. Method

5.1 Finding Initial Conditions

In the absence of knowledge of current velocities of the galaxies, an orbit integration scheme is used to derive the initial conditions. Numerous simple 2-body, time-reversed simulations are run from current positions for 1.5 *Gyrs*, with varying relative velocities. This is done to find the velocity values that best replicate the expected interaction history. The velocities are relative as NGC 5258, which is placed at the origin, has zero velocity in each direction.

Within these 2-body simulations, each galaxy is treated exclusively as a DMH and modelled as a single particle. Newtonian gravity is not included, so the potential DMH and dynamical friction from each galaxy are the only forces present in the simulation. Their equations of motion for the galaxies are:

$$\begin{aligned}\ddot{\mathbf{x}}_{NGC5257} &= -\nabla\phi_{NGC5258} + \mathbf{f}_{DF_{NGC5258}}, \\ \ddot{\mathbf{x}}_{NGC5258} &= -\nabla\phi_{NGC5257} + \mathbf{f}_{DF_{NGC5257}},\end{aligned}\tag{5.1}$$

where ϕ is the DMH potential and \mathbf{f}_{DF} is the acceleration caused by dynamical friction. These simplifications decrease the computational complexity of the simulation, which is crucial due to the large volume of them expected to be run.

Information on star formation history and stellar population ages [31] indicates that the pericentre of the previous close encounter of Arp 240 occurs between 0.2 – 0.3 *Gyrs* ago. The pericentre is the point, during a close encounter, when the two galaxies are nearest each other. In order to produce the distinct morphological features observed in the system, the pericentre separation is expected to have a value between 10 – 40 *kpc*.

The result that best fits the above conditions is used to find the initial parameters for the full interaction simulation. The position between the galaxies, and the velocities, is again made relative by placing NGC 5258 at the origin with zero velocity in all directions.

Inaccuracies are expected with the initial conditions as the model used in these simulations does not take into account tidal stripping of each galaxy. This has been previously found, in Tepper-Garcia *et al.*, 2020 [47], to affect the pericentre separation and its time of occurrence in simulations of a similar manner.

5.2 Simulating the Interaction

Each galaxy is first simulated in isolation to ensure that it remains stable for an extended period of time and that morphological features are not induced by any other processes. These isolated galaxies are subsequently inserted into the full interaction simulation. The interaction is modelled until its conclusion, allowing for the futures of both galaxies in the system to be seen, as well as giving the ability to analyse how their morphological features change with time.

Initially, a preliminary simulation is run to ensure that the results are as expected. Within this simulation, a combination of a halo potential and dynamical friction is used, in addition to massless disk particles. This allows for simple results to be produced as quickly as possible.

Assuming the preliminary simulations show acceptable results, more detailed simulations can be constructed. This would involve massive disk particles, as well as implementing a live DMH for each galaxy. It is expected that these simulations will give a more accurate interpretation of the interaction.

Snapshots containing information on all particles are saved periodically during the simulation, allowing for the inspection and analysis of the galaxies throughout their interaction.

6. Results & Analysis

6.1 Determining Initial Conditions

Trial time-reversed simulations indicated that NGC5257 would have to be travelling unrealistically fast in order to have an acceptable previous close encounter, due to the current observed separation of the galaxies being $\sim 600\text{ kpc}$ [31]. To overcome this assumed error, the magnitude of the separation between the galaxies was reduced and varied for each simulation conducted.

The best result from the orbit integration scheme, shown in Figure 6.1, was used to obtain initial conditions for the interaction simulation. It was selected based on its pericentre information, as well as ensuring that the path included a single close encounter and the system didn't appear to be orbiting each other.

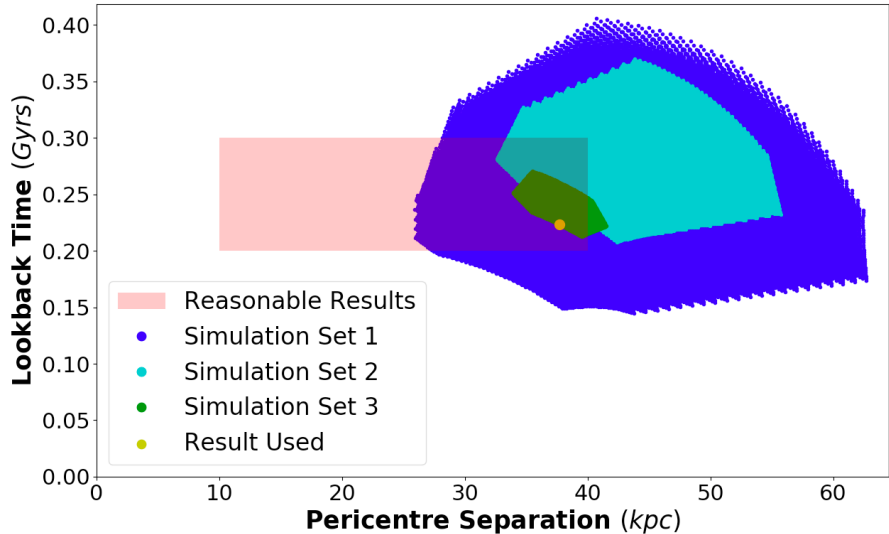


Figure 6.1: Pericentre separation and time of occurrence, looking back from current time, of a previous close encounter for all simulations conducted during the orbit integration scheme.

Information on the time-reversed simulation used can be seen in Figure 6.2. The close encounter had a pericentre separation of 37.73 kpc at a lookback time of 0.2234 Gyrs .

Table 6.1 outlines the initial conditions of NGC 5257, for the interaction simulation.

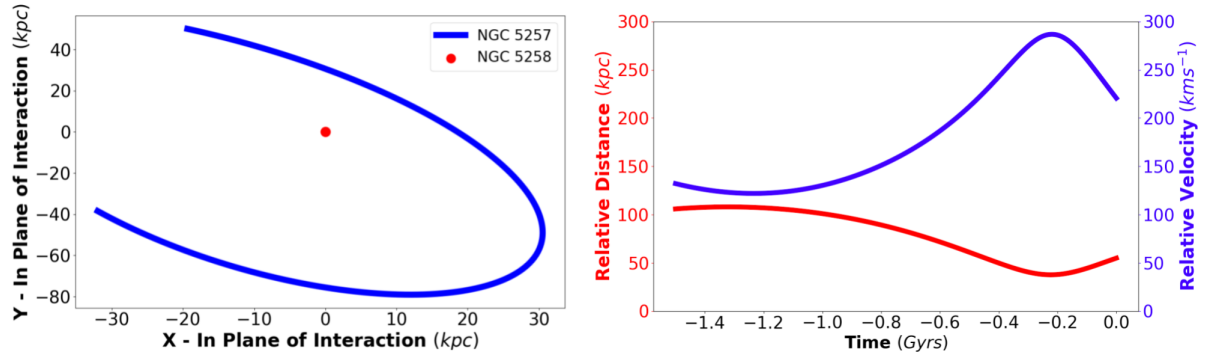


Figure 6.2: Left: The relative path of NGC 5257 about NGC 5258 during the time-reversed simulation used to find initial conditions of the interaction. The path is shown on the 2D plane of the interaction. NGC 5258 is placed at the origin at every step. Right: The relative distance and velocity between the galaxies during the time-reversed simulation. A single close encounter is observed.

Vector	X	Y	Z	Units
Relative Position	-32.0	-38.4	-93.4	kpc
Relative Velocity	61.5	-117.0	1.5	$km s^{-1}$

Table 6.1: Initial conditions for NGC 5257, used at the beginning of the full interaction simulation. NGC 5258 is placed at the origin with no velocity.

6.2 Preliminary Simulation

Galaxy component parameters used in the simulation were taken from observational data (stated in Appendix D). Both galaxy disks contained 1500 particles and were given a spin that ensures they have a prograde passage. Retrograde passages were not able to recreate observed morphological features (See Appendix E).

6.2.1 Isolation Simulations

Prior to the full simulation, each galaxy was simulated in isolation for 1 *Gyr*. Figure 6.3 shows the results of these simulations, with the disks remaining stable and no morphological features being induced. They were subsequently used in the interaction simulation.

The nearest neighbour density, as seen in plots throughout this section, were calculated by finding the number of other bodies within a $2.5\ kpc$ radius of each body. This value was chosen as it best demonstrates the density fluctuations.

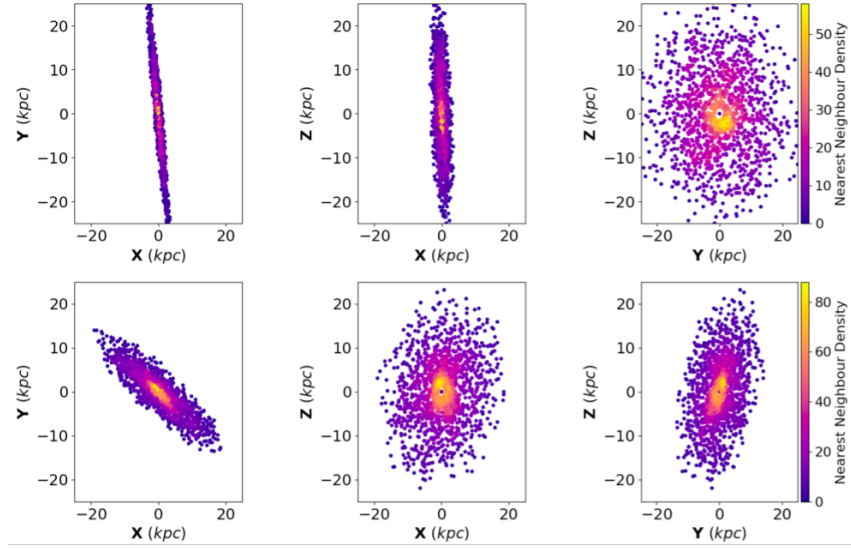


Figure 6.3: Nearest neighbour density plots for both galaxies at the end of their isolation simulations. Top: NGC 5257. Bottom: NGC 5258.

6.2.2 Full Interaction Simulation

The preliminary simulation was run for 6 *Gyrs*. Information on the path of the galaxies can be seen in Figure 6.4. Three close encounters can be seen during the interaction, with the first having a pericentre separation of 34.78 *kpc* at a time of 1.15 *Gyrs* into the simulation. This is 0.127 *Gyrs* sooner, and 2.95 *kpc* closer, than expected in the time-reversed simulation. Newtonian gravity is not included in the time-reversed simulations, accounting for the differences.

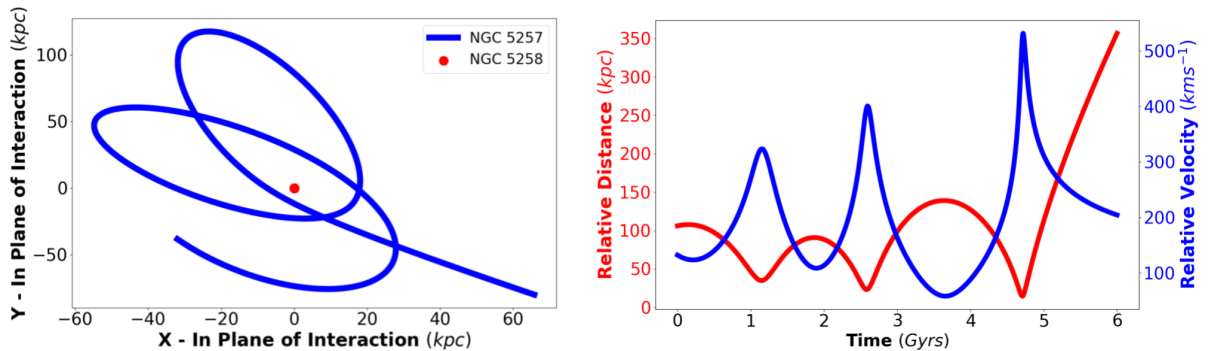


Figure 6.4: Left: The relative path of NGC 5257 about NGC 5258, which is continually placed at the origin, during the preliminary simulation. The path is shown on the 2D plane of the interaction. Only the first 5 Gyrs of the path is shown, as after this the galaxies are gravitationally unbound from one another. Right: The relative positions and velocities of the galaxies during the preliminary simulation.

Figure 6.5 presents the density perturbations of the disk at 1.5 *Gyrs* into the interaction, equivalent to the current observational time of the interaction. General spiral structure is seen

in both galaxy disks, reminiscent to that of observations in Figure 3.1. NGC 5257's disk is less similar to observations, being perturbed in a different direction.

Figure 6.6 shows the density perturbations of the system in the line of sight (LoS) view from Earth, showing no resemblance to the observed view of the system. In addition, the relative LoS velocity of NGC 5257 in the simulation is -28.3 km s^{-1} , compared to the observed value of -1 km s^{-1} [31].

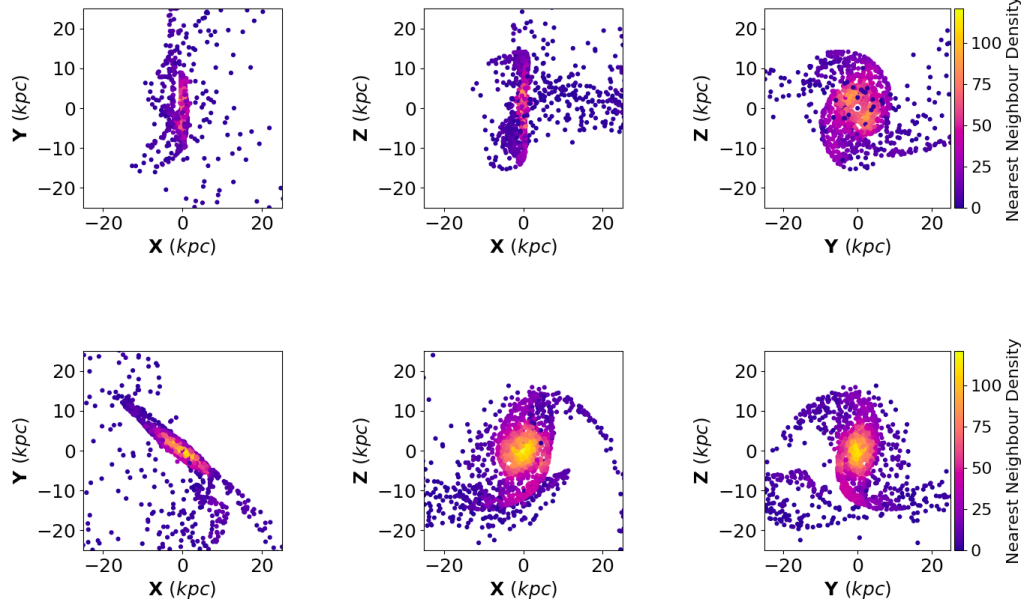


Figure 6.5: Nearest neighbour density plots for the galaxy disks 1.5 Gyrs into the simulation.
Top: NGC 5257. Bottom: NGC 5258.

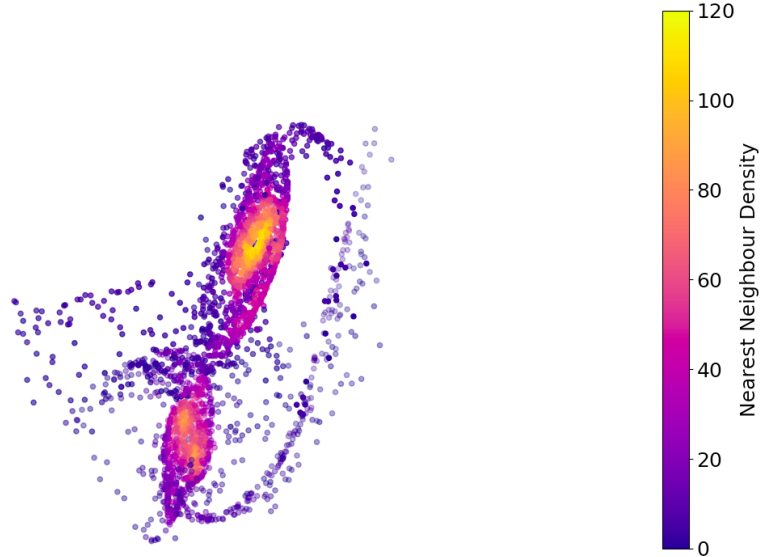


Figure 6.6: Nearest neighbour density plots for the 'Line of Sight' view of the whole system 1.5 Gyrs into the simulation. Left: NGC 5257. Right: NGC 5258. Line of Sight view is found by aligning the 3D plot view with a line pointing towards Earth in the simulation space.

Instead of viewing the interaction in the LoS, a best fit view, attempting to replicate Figure 3.1, is used in Figure 6.7 to observe the system 1.5 *Gyrs* into the simulation. A tidal bridge is visible between the galaxies, predominantly being made up of matter from NGC 5257. Tidal tails are observed in both simulated galaxies, with NGC 5257's being thicker and extending further than NGC 5258's. NGC 5257's tail is not seen in observations as prominently as it is in the simulation.

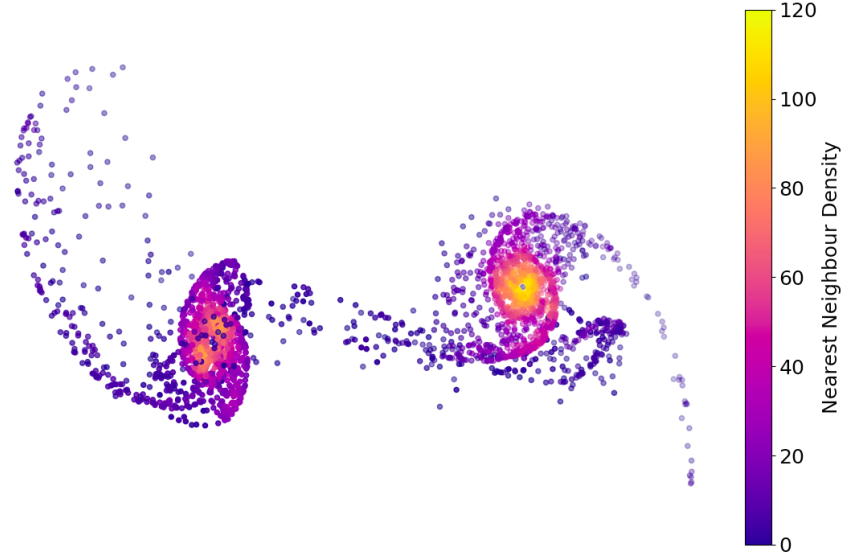


Figure 6.7: Nearest neighbour density plots for the 'Best Fit' view of the whole system 1.5 *Gyrs* into the simulation. Left: NGC 5257. Right: NGC 5258. Best fit view is orientated in a 3D plot to best replicate the view in Figure 3.1.

Figure 6.8 shows the origin of all disk particles and their current position. It can be observed that the majority of tidally stripped particles originated at further distances from the galactic centres. In addition, NGC 5258 appears to have stripped more particles than NGC 5257. The bridge is made up predominantly of NGC 5257 particles. NGC 5257's tidal tail contains particles predominantly from the outer regions of the disk, whereas NGC 5258's tail contains exclusively outer disk particles.

The rotation curves of the simulated galaxies, at observed time, can be seen in Figure 6.9. The absence of a modelled galactic bulge causes the rotation curve at small radii to differ significantly from its expected shape. At farther radii, the radial velocity is lower than expected from observational data [31].

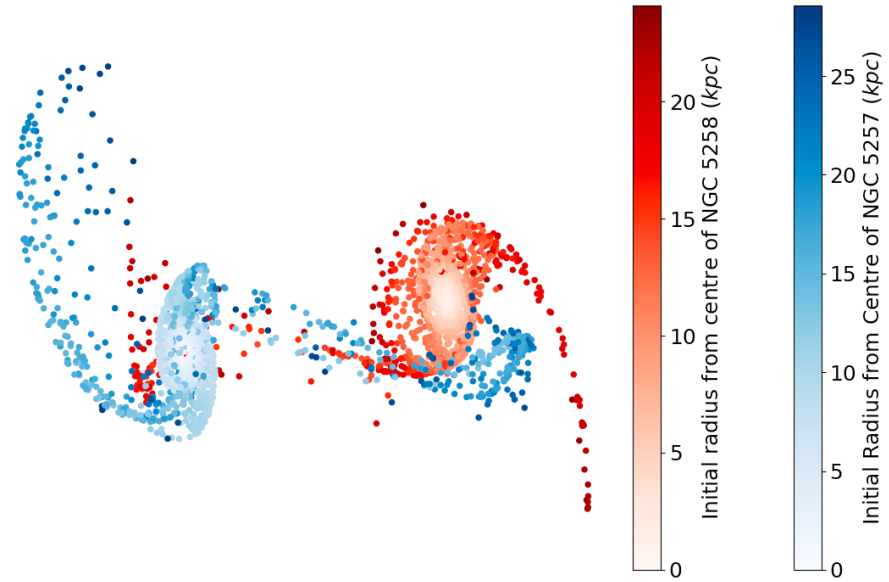


Figure 6.8: A best fit view of the system 1.5 Gyrs into the simulation, showing the location of all disk particles, whose colours correlates to their initial position in their original host galaxy's disk.

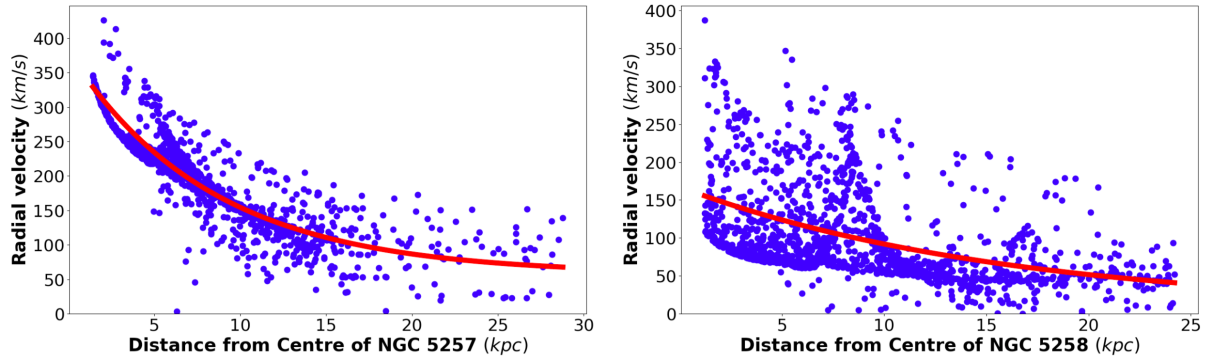


Figure 6.9: The rotation curve for each galaxy, 1.5 Gyrs into the simulation, plotted from snapshot data. A line of best fit is included for convenience. Left: NGC 5257. Right: NGC 5258.

Figure 6.10 displays how the spiral structure in each galaxy's disk evolves after the initial close encounter. It can be seen that within 0.7 Gyrs the spiral arms disperse in both galaxies.

Figure 6.11 shows how the system's morphological features, created by the first close encounter, evolve with time. The bridge's thickness decreases as matter is taken by the galaxies. NGC 5257's tidal tail becomes clearly separated from the rest of the galaxy, elongating away. NGC 5258's tail appears more reminiscent of a counterarm, as it continues to rotate with the disk and indicates a future recombination. This could not be observed due to the occurrence of the second close encounter.

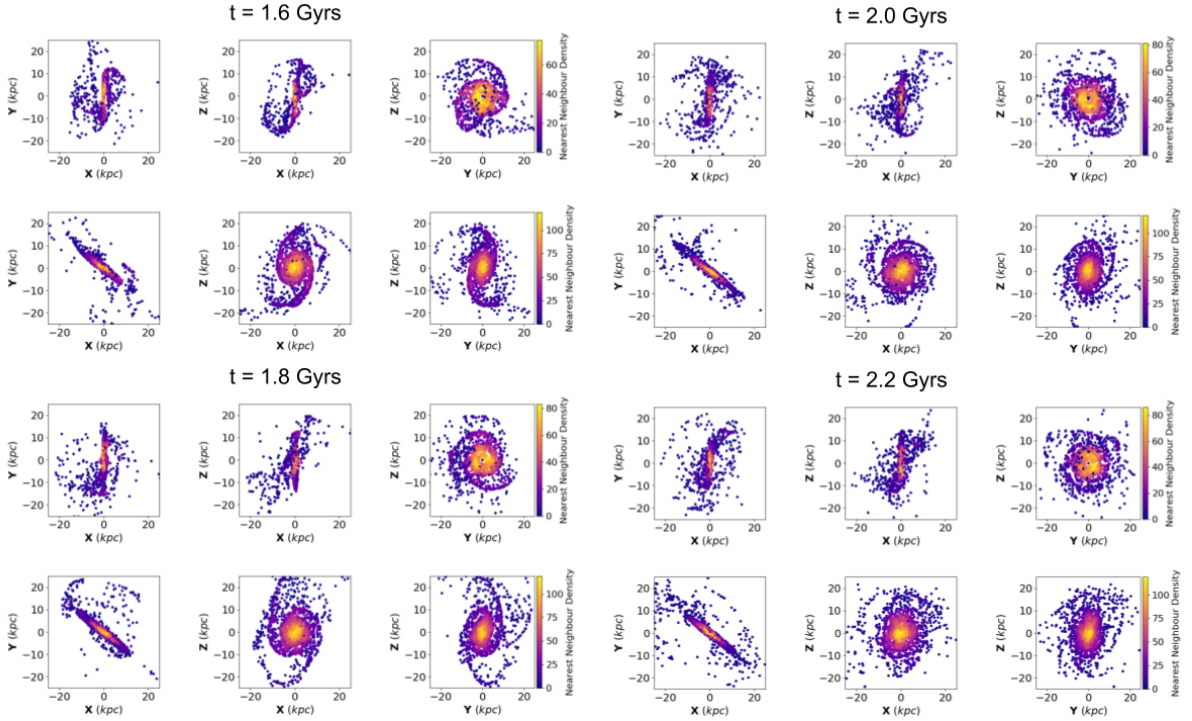


Figure 6.10: A set of nearest neighbour density plots for the disks of each galaxy in the simulation at subsequent snapshots following the first close encounter. Top: NGC 5257, Bottom: NGC 5258 (For each individual plot).

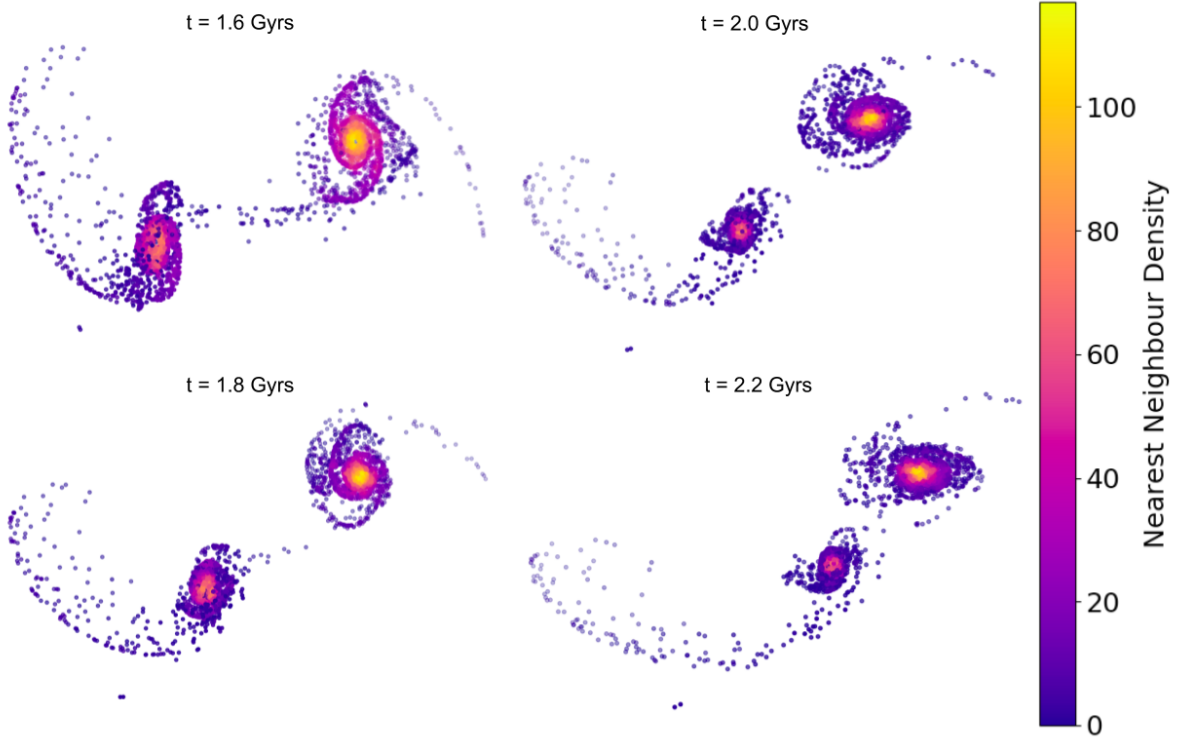


Figure 6.11: A set of best fit view, nearest neighbour density plots for the system in the simulation at subsequent snapshots following the first close encounter. Left: NGC 5257, Right: NGC 5258 (For each individual plot).

Following the second close encounter, broad, short-lived (~ 0.2 Gyrs lifespan) spiral arms are observed in NGC 5258's disk. After this, and until the simulation's conclusion, no obvious disk structure or morphological features are observed in the system, with NGC 5257 appearing to become elliptical (See Appendix F). Figure 6.12 shows the final positions of all disk particles, relative to their initial positions. It is clear to see that both galaxies have stripped considerable matter from each other, with the majority originating the outer regions of the disks. In addition, large amounts of matter are isolated from the galaxies by the interaction's conclusion, showing no clear structure.

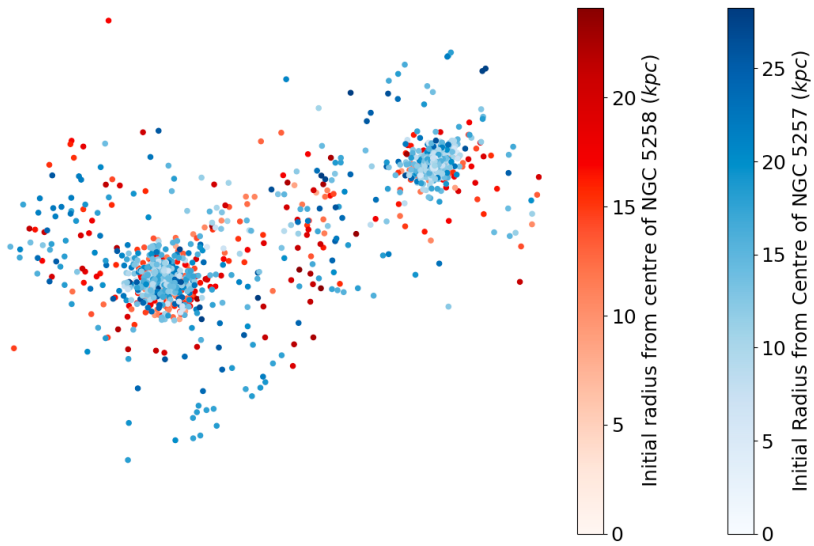


Figure 6.12: A best fit view of the system at the simulation's end, showing the location of all disk particles, whose colours correlate to their initial position in their original host galaxy's disk.

6.3 Live Dark Matter Halo Simulations

As previously explained in Section 4.4, issues occurred when combining a live DMH and disk in simulations. This was demonstrated through a trial isolation simulation conducted with NGC 5258 (See Appendix D for modelling parameters), with a reduced disk radius. The simulation was 1 Gyr long, with 300 disk particles and 1000 halo particles. The densities of the disk at the start and end of the simulation can be seen in Figure 6.13. The disk is seen to be unstable, even with corrections, becoming elliptical by the simulation's end.

In order to assess the accuracy of the preliminary simulation results, a reduced simulation was conducted with live DMHs, using the same initial conditions and parameters as in preliminary simulation (See Appendix D). Each galaxy was modelled with a central particle, containing the all the baryonic mass, and a live halo consisting of 1000 particles. Figure 6.14 displays the paths of the central particles during the 6 Gyr simulation. The system appears to merge, seen

from the multiple, tight orbits, as expected [33]. NGC 5257's central particle diverges towards the simulation's end due to a gravitational singularity, as a softening parameter was not included in the simulation.

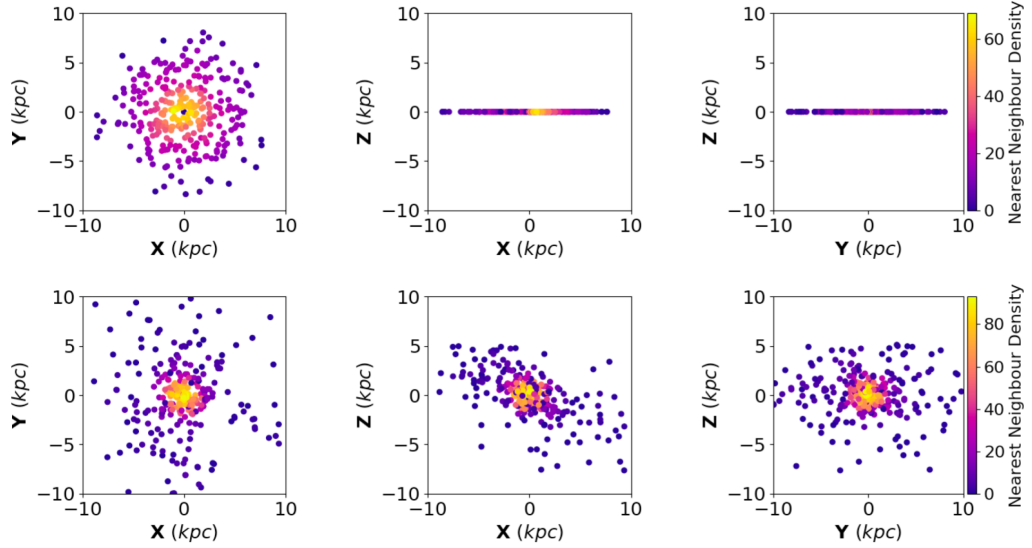


Figure 6.13: Nearest neighbour density plot for NGC 5258's disk particles before (top) and after (bottom) a 1 Gyr live DMH trial isolation simulation. The disk is set in the X-Y plane for clarity. Credit: Amy Hewitt.

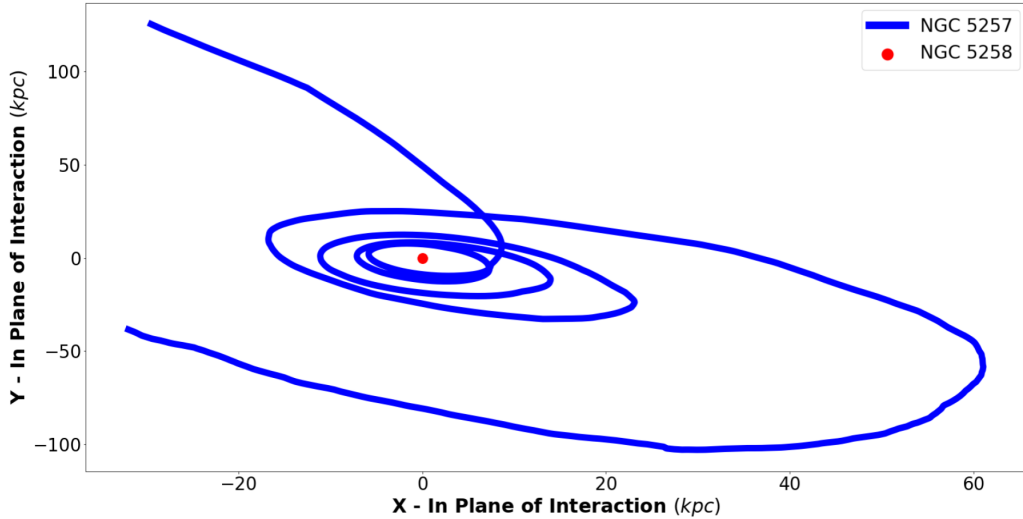


Figure 6.14: The relative path of NGC 5257's central baryonic particle about NGC 5258's, in a 6 Gyr simulation including live DMHs. It is shown on a 2D plane of the interaction and NGC 5258 is placed at the origin at every step. Credit: Amy Hewitt.

7. Discussion

7.1 Technical Limitations

A key issue encountered during this investigation was the substantial run-times of simulations on the hardware available, even with implemented functions to reduce computational complexity. Furthermore, Python is comparatively slower than other programming languages, such as C [48], also impacting run-times. This restricted the value of N within the simulations, decreasing their accuracy and reducing the visual resolution when observing morphological features of the interaction.

7.2 Initial Conditions

The irregularity of the Arp 240's current separation, discussed in Section 6.1, could suggest errors in the observational data used [31]. However, the rest of the data appeared consistent for modelling the galaxies, indicating a possible outlier.

The number of simulations conducted in the orbit integration scheme was not as large as desired. The volume required in order to iterate over all reasonable velocities was too substantial to be carried out within the time frame of the study. This resulted in a derivation of initial conditions from a simulation that may not best fit the interaction. The volume of simulations required could be reduced by introducing the preliminary condition that each time-reversed simulation is only conducted if the initial LoS velocity is comparable with the current observed value [31].

7.3 Preliminary Simulation

Interaction features occurring predominantly along the line of sight posed some difficulty in accurately replicating the observation of the galaxies within the simulation. The LoS view, in the simulation, was clearly inconsistent with the observed view. In addition, the relative LoS velocities at current time differed to that of expected values [31].

A success of the simulation was the visual recreation of the observed morphological features. General features were recreated, with the exception of NGC 5258's supposed counterarm instead of a tail. The features deviated from their expected appearance when analysed in more detail. NGC 5257's tidal tail was sparse and larger than expected, whereas NGC 5258's counterarm was thinner than observations. Finally, their tidal bridge was sparse and short-lived. An insufficient number of disk particles, reducing the morphological features' resolution, could account for the observed deviations.

The rotation curves for both galaxies are significantly below the observed curves [31]. In addition, the system does not result in a merger as expected [33], both furthering the evidence that this simulation was inaccurate. Tidal stripping of the halo is not included when using a potential DMH model, plausibly accounting for the unexpected interaction conclusion.

These results imply that there must be some degeneracy between different initial conditions, and galactic modelling parameters, in order to have reproduced Arp 240's morphological features with an inaccurate orbit.

7.4 Live Dark Matter Halo Simulations

Galaxy disks were unstable when combined with a live DMH. Incorporating adjustments to ensure the virial theorem was met reduced the instability but did not correct the issue. In order to avoid this the halo and the disk should instead be created in conjunction with each other.

The path of the galaxies' when modelled with live DMHs did not replicate that of the preliminary simulation, orbiting each other less and instead merging. These simple results suggest that using a live DMH will produce results consistent with those expected of the interaction.

7.5 Program Performance

Discrepancies in the simulation's conclusions imply that the simplified DMH model is inaccurate. It is theorized that the model of dynamical friction used is not functioning as expected, with the coulomb logarithm (Equation 4.6) being the likely culprit. Semczuk *et al.*, 2018 [10], compared simulations with a simplified halo to those with a live halo, adjusting the value of ϵ until the paths were equivalent. This was not carried out during this study due to time constraints and could explain the contradictory path seen in the preliminary simulation.

This incorrect implementation of dynamical friction devalues all previous simulations that use the model, including the preliminary interaction simulation and those conducted to obtain initial conditions, rendering their results unreliable. However, the preliminary simulation could be said to still be valid, as it is consistent with the incorrectly calibrated dynamical friction used to find its initial conditions.

8. Conclusion

This investigation aimed to develop a basic N-Body code, that could be used to model known galaxy interactions, and use it to simulate a novel, observed interacting system. This was done to help understand the formation of morphological features during galactic close encounters and further computational resources in the field.

A relatively computationally efficient N-Body code able to basically model interactions was successfully developed. However, results of this investigation imply that the program, in its current state, is not sufficient to accurately model an observed galactic interaction in a detailed manner. Whilst being able to model large N simulations faster than a brute-force method, the program continues to experience long run-times, likely due to the chosen programming language.

Arp 240 was the chosen system to model due to the obvious morphological features observed. The initial conditions were derived from observational data and sets of time-reversed simulations, which made use of a reduced galaxy model. The simulations performed covered a small amount of the parameter space, due to time constraints, resulting in the use of unproven best-fit initial conditions for the interaction. Observed features in the galaxies were able to be recreated in a preliminary simulation, using a simplified model consistent with that used to find initial conditions. Simulating the interaction with a live DMH model produced contradictory results to that of the preliminary simulation but was in agreement with predictions. It is theorised the inaccuracies of the preliminary simulation is the result of improperly calibrated dynamical friction in the simplified DMH model, also resulting in unreliable initial conditions.

8.1 Future Work

With regards to the program developed in this study, it may be preferable to convert to the C programming language in order to decrease the run time of simulations. In addition, implementing further algorithms to reduce computational complexity will aid in this too.

Following the progress of modelling a novel interaction, the dynamical friction model should first be correctly calibrated for the Arp 240 galaxies in the simulation. After this, a larger volume of time-reversed simulations for the orbit integration scheme should be conducted in order

to determine the most accurate initial conditions. Additional research on the history of the Arp 240 galaxies should be done to further the constraints on their feasible paths prior to the first close encounter.

Subsequently, simulations of the interaction should be conducted with both a live and potential DMH. These simulations should contain a large N to ensure accurate results and visual clarification to a good resolution. After this, the interaction should be simulated using a pre-existing, comprehensive N-Body code, such as GADGET-2 [5]. Comparisons can then be made across the simulations conducted, allowing for the accuracy of the written N-Body code to be determined.

Acknowledgements

I would like to thank the supervisors of this study, Professor Clare L. Dobbs and Dr Steven Rieder, for their continual and knowledgeable support over the course of this investigation.

I would also like to thank my partners in this study, Amy L. Hewitt and Mattias H. Blake, for their co-operation and resourcefulness throughout. The majority of the project was done collaboratively, with the workload being equally split. Towards the latter stages, Amy focused on implementing the Barnes-Hut algorithm and stabilizing galaxy disks when using a live DMH. Mattias and I worked on implementing dynamical friction and creating the orbit integration scheme. I was also responsible for determining relevant information on Arp 240, as well as writing the majority of analysis code used.

Additionally, I would like to extend my gratitude to Dr Isaura Fuentes-Carrera and Dr Marcin Semczuk for their time and patience when contacted.

Appendix A

Galactocentric Rest Frame

The galactocentric rest frame refers to the Cartesian reference frame where the origin lies on the galactic centre of the Milky Way. The x-axis points from the Sun towards the galactic centre, the y-axis points in the direction of the Sun’s rotation about the galactic centre, and the z-axis points towards the Galactic north pole, perpendicular to the plane of the Milky Way’s disk.

The distance between the Sun and the galactic centre is $R_0 = 8.0 \text{ kpc}$ [49], allowing for a vector between the Sun and galactic centre to be known. This then allows for simple conversion to the galactocentric rest frame.

Appendix B

Accessing Written Code

The code written (for the orbit integration scheme, simplified halo model and analysis functions) during this investigation can be found on a personal GitHub repository [50]. More information on how to download and operate the program can be found in the README.md file within the repository.

The code's development was done using an IDE (Integrated Development Environment), for ease. Because of this the majority of functions are not operated through command line arguments, instead parameters inside the file are changed before being run. After this, functions can be run from the command line, an example being:

```
python NBody.py
```

Work should be done following this study to include command line options for all functions.

Appendix C

Downloading and Operating HaloGen

The source code for AMUSE can be found on its GitHub repository [51], where instructions can be found outlining the installation process and any other requirements, such as having a C/C++ compiler.

In short, the simplest way, if using Mac or Linux, is:

```
pip install amuse
```

Alternatively, the source code can be downloaded directly from GitHub and compiled using a Makefile.

Once installed, HaloGen can be used to generate stable live DMHs. An example command line to generate an NFW halo is as follows.

```
halogen4muse -a 1 -b 3 -c 1 -M 1000 -rs 5 -rcutoff 50 -name NFW
```

This will generate an NFW profile with parameters: $M_{tot} = 1000 M_\odot$, $R_s = 5 kpc$ and $R_{cutoff} = 50 kpc$. a , b and c represent α , β and γ , respectively, which are used in the NFW profile equation within the code, seen in Equation C.1.

$$\rho(r) = \frac{\rho_0}{\left(\frac{r}{R_s}\right)^\gamma \left(1 + \left(\frac{r}{R_s}\right)^\alpha\right)^{\left(\frac{\beta-\gamma}{\alpha}\right)}} \quad (\text{C.1})$$

Appendix D

Galactic Modelling Parameters

Table D.1 outlines the parameters for all galactic components within the simulations.

Component	Property	Value	Units
NGC 5257 Baryonic Disk	Mass	3.58×10^{10}	M_{\odot}
	Maximum Radius	28.86	<i>kpc</i>
	Maximum Velocity	325	kms^{-1}
NGC 5257 Dark Matter Halo	Mass	1.12×10^{11}	M_{\odot}
	Concentration	6.1	-
	Scale Radius	4.39	<i>kpc</i>
	Virial Radius	26.8	<i>kpc</i>
NGC 5258 Baryonic Disk	Characteristic Density	0.05	M_{\odot}/pc^3
	Mass	4.06×10^{10}	M_{\odot}
	Maximum Radius	24.22	<i>kpc</i>
	Maximum Velocity	320	kms^{-1}
NGC 5258 Dark Matter Halo	Mass	2.46×10^{11}	M_{\odot}
	Concentration	4.3	-
	Scale Radius	8.30	<i>kpc</i>
	Virial Radius	35.4	<i>kpc</i>
	Characteristic Density	0.71	M_{\odot}/pc^3

Table D.1: NGC 5257 and NGC 5258's modelling parameters, taken and calculated from observational data [31].

Appendix E

Retrograde Passages

Through test simulations to the current time of the interaction, it was seen that retrograde passages do not recreate observed, or any, morphological features. The galaxy disks, during a retrograde passage for both galaxies, at current time can be seen as featureless in Figure E.1.

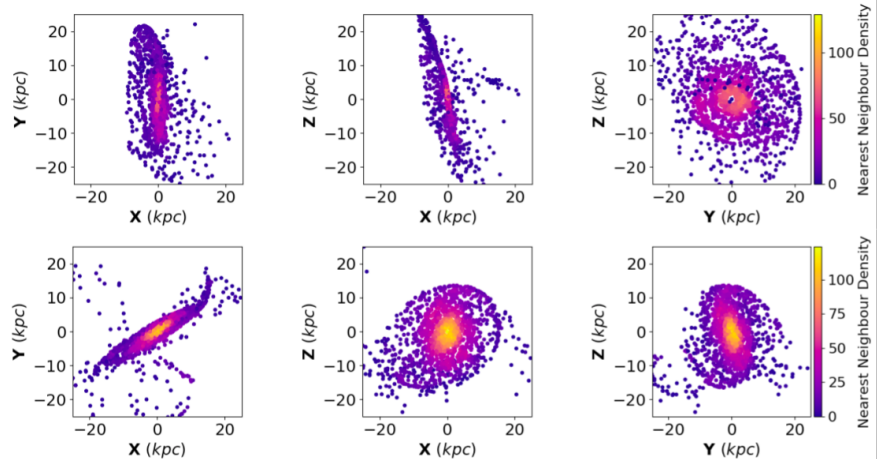


Figure E.1: Nearest neighbour density plots for the galaxies at the current time of the interaction, for retrograde passages. Top: NGC5257. Bottom: NGC5258.

Appendix F

Post Second Close Encounter Morphology

Figure F.1 shows how each galaxy disk looks, following the second close encounter. Figure F.2 shows the lack of morphological features between the galaxies in the same snapshot.

Alternatively, a video of every consecutive snapshot taken during the simulation can be seen using the following link:

<https://www.youtube.com/watch?v=uEZ3Kmc94NA>.

Each graph takes the same form as Figure F.1, with NGC 5257 being the top set of plots and NGC 5258 being the bottom set. This allows for the entire interaction to be seen at once.

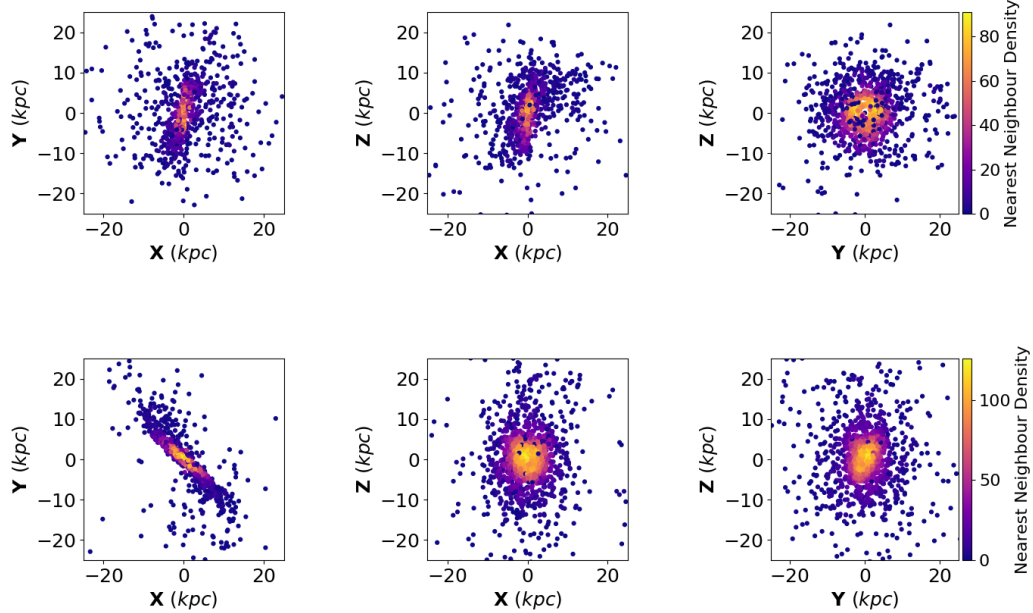


Figure F.1: Nearest neighbour density plots for the galaxy disks *3.5 Gyrs* into the simulation, following the second close encounter. Top: NGC 5257. Bottom: NGC 5258.

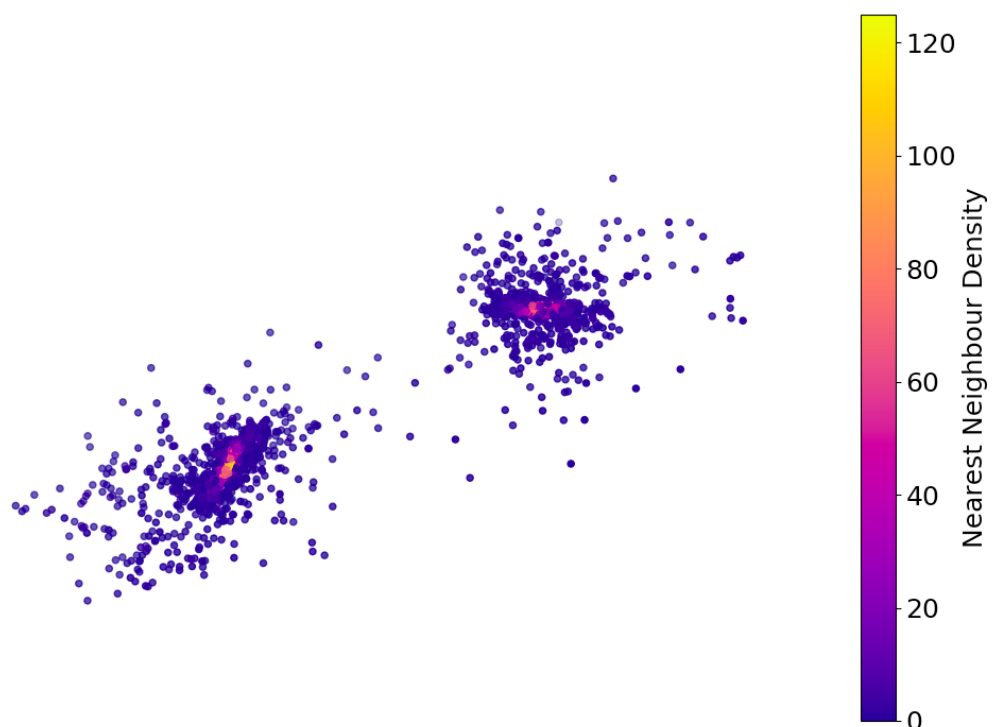


Figure F.2: Nearest neighbour density plots for the 'Best Fit' view of the whole system 3.5 Gyrs into the simulation. Left: NGC 5257. Right: NGC 5258.

Bibliography

- [1] M. S. Seigar and P. A. James, “A test of arm-induced star formation in spiral galaxies from near-infrared and $H\alpha$ imaging,” *Monthly Notices of the Royal Astronomical Society*, vol. 337, pp. 1113–7, 2002.
- [2] R. Buta, “Secular evolution of galaxies,” *XXIII Canary Islands Winter School of Astrophysics*, p. 155, 2013.
- [3] C. Lintott, K. Schawinski, S. Bamford, A. Slosar, K. Land, D. Thomas, E. Edmondson, K. Masters, R. C. Nichol, J. M. Raddick, A. Szalay, D. Andreescu, P. Murray, and J. Vandenberg, “Galaxy zoo 1: data release of morphological classifications for nearly 900 000 galaxies,” *Monthly Notices of the Royal Astronomical Society*, vol. 140, pp. 166–78, 2011.
- [4] A. Toomre and J. Toomre, “Galactic bridges and tails,” *The Astrophysical Journal*, vol. 178, pp. 623–66, 1972.
- [5] V. Springel, “The cosmological simulation code GADGET-2,” *Monthly notices of the royal astronomical society*, vol. 364, pp. 1105–34, 2005.
- [6] H. Salo and E. Laurikainen, “N-body model for m51—i. multiple encounter versus single passage?”, *Monthly Notices of the Royal Astronomical Society*, vol. 319, no. 2, pp. 377–92, 2000.
- [7] C. L. Dobbs, C. Theis, J. E. Pringle, and M. R. Bate, “Simulations of the grand design galaxy m51: a case study for analysing tidally induced spiral structure,” *Monthly Notices of the Royal Astronomical Society*, vol. 403, no. 2, pp. 625–45, 2010.
- [8] B. S. Koribalski and Á. R. López-Sánchez, “Gas dynamics and star formation in the galaxy pair ngc 1512/1510,” *Monthly Notices of the Royal Astronomical Society*, vol. 400, no. 4, pp. 1749–67, 2009.
- [9] C. Horellou and B. Koribalski, “Stars and gas in the very large interacting galaxy ngc 6872,” *Astronomy & Astrophysics*, vol. 464, no. 1, pp. 155–65, 2007.
- [10] M. Semczuk, E. L. Lokas, J. Salomon, E. Athanassoula, and E. D’Onghia, “Tidally induced morphology of M33 in hydrodynamical simulations of its recent interaction with M31,” *The Astrophysical Journal*, vol. 864, pp. 34–55, 2018.
- [11] C. Dobbs and J. Baba, “Dawes review 4: Spiral structures in disc galaxies,” *Publications of the Astronomical Society of Australia*, vol. 31, 2014.

BIBLIOGRAPHY

- [12] L. S. Sparke and J. S. Gallagher, *Galaxies in the Universe: An Introduction*. Cambridge University Press, 2000.
- [13] G. R. Blumenthal, S. M. Faber, J. R. Primack, and M. J. Rees, “Formation of galaxies and large-scale structure with cold dark matter,” *Nature*, vol. 311, pp. 517–25, 1984.
- [14] E. P. Hubble, “Extra-galactic nebulae,” *Astrophysical Journal*, vol. 64, pp. 321–69, 1926.
- [15] S. van den Bergh, “The origin of lenticular galaxies,” *Journal of the Royal Astronomical Society of Canada*, vol. 73, pp. 198–202, 1979.
- [16] J. Loveday, “The apm bright galaxy catalogue,” *Monthly Notices of the Royal Astronomical Society*, vol. 278, pp. 1025–48, 1996.
- [17] S. M. Alladin and S. N. Hasan, “Interactions and mergers of galaxies,” *Resonance*, vol. 12, pp. 13–26, 2007.
- [18] C. C. Lin and F. H. Shu, “On the spiral structure of disk galaxies, ii. outline of a theory of density waves,” *Proceedings of the National Academy of Sciences of the United States of America*, vol. 55, no. 2, pp. 229–34, 1966.
- [19] A. Toomre, “On the gravitational stability of a disk of stars,” *The Astrophysical Journal*, vol. 139, pp. 1217–38, 1964.
- [20] K. R. V. Casteels, S. P. Bamford, R. A. Skibba, K. L. Masters, C. J. Lintott, W. C. Keel, K. Schawinski, R. C. Nichol, and A. M. Smith, “Galaxy zoo: quantifying morphological indicators of galaxy interaction,” *Monthly Notices of the Royal Astronomical Society*, vol. 429, pp. 1051–65, 2013.
- [21] N. Tashpulatov, “The tidal effect and the formation of bridges and tails in galaxies. ii. formation of tails in interacting galaxies during close approaches.,” *Soviet Astronomy*, vol. 14, pp. 227–91, 1970.
- [22] N. Tashpulatov, “The tidal effect and the formation of bridges and tails in galaxies. i. tidal formation of linear bridges between galaxies.,” *Translated from Astronomicheskii Zhurnal*, vol. 46, pp. 1236–46, 1969.
- [23] C. Dobbs, “Star formation in galaxies: the role of spiral arms,” *Proceedings of the IAU Symposium No. 298, ”Setting the scene for Gaia and LAMOST”*, 2013.
- [24] Y. Yoon, M. Im, G.-H. Lee, S.-K. Lee, and G. Lim, “Observational evidence for bar formation in disk galaxies via cluster-cluster interaction,” *Nature Astronomy*, vol. 3, 2019.
- [25] NASA, ESA, The Hubble Heritage Team (STScI/AURA)-ESA/Hubble Collaboration, and A. Evans, “Eso 77-14.” <https://www.spacetelescope.org/images/heic0810ao/>, 2008. Last accessed 09 April 2020.
- [26] NASA, ESA, and The Hubble Heritage Team (STScI/AURA), “Barred spiral galaxy ngc 1300.” <https://hubblesite.org/contents/media/images/2005/01/1636-Image.html>, 2005. Last accessed 09 April 2020.

BIBLIOGRAPHY

- [27] E. Holmberg, “On the clustering tendencies among the nebulae. ii. a study of encounters between laboratory models of stellar systems by a new integration procedure,” *Astrophysical Journal*, vol. 94, pp. 385–95, 1941.
- [28] J. Barnes and P. Hut, “A hierarchical O (NlogN) force-calculation algorithm,” *Nature*, vol. 324, pp. 446–449, 1986.
- [29] W. Dehnen, “A fast multipole method for stellar dynamics,” *Computational Astrophysics and Cosmology*, vol. 1, 2014.
- [30] P. Teuben, “The stellar dynamics toolbox nemo,” *Astronomical Data Analysis Software and Systems IV, ASP Conference Series*, vol. 77, pp. 398–401, 1995.
- [31] I. Fuentes-Carrera, M. Rosado, P. Amram, E. Laurikainen, H. Salo, J. Gomez-Lopez, H. Castaneda, A. Bernal, and C. Balkowski, “Kinematics and dynamics of the luminous infrared galaxy pair NGC 5257/58 (Arp 240),” *Astronomy & Astrophysics*, vol. 621, 2019.
- [32] NASA, ESA, The Hubble Heritage Team (STScI/AURA)-ESA/Hubble Collaboration, and A. Evans, “NGC 5257, NGC 5258.” <https://spacetelescope.org/images/heic0810at/>, 2008. Last accessed 30 March 2020.
- [33] D. Iono, M. S. Yun, and P. T. P. Ho, “Atomic and molecular gas in colliding galaxy systems. i. the data,” *The Astrophysical Journal Supplement Series*, vol. 158, pp. 1–37, 2005.
- [34] G. C. Privon, J. E. Barnes, A. S. Evans, J. E. Hibbard, M. S. Yun, J. M. Mazzarella, L. Armus, and J. Surace, “Dynamical modeling of galaxy mergers using identikit,” *The Astrophysical Journal*, vol. 771, pp. 120–35, 2013.
- [35] J. E. Barnes and J. E. Hibbard, “Identikit 1: A modeling tool for interacting disk galaxies,” *The Astronomical Journal*, vol. 137, pp. 3071–90, 2009.
- [36] A. J. Holincheck, J. F. Wallin, K. Borne, L. Fortson, C. Lintott, A. M. Smith, S. Bamford, W. C. Keel, and M. Parrish, “Galaxy zoo: Mergers – dynamical models of interacting galaxies,” *Monthly Notices of the Royal Astronomical Society*, vol. 459, p. 720–45, 2016.
- [37] J. F. Navarro, C. S. Frenk, and S. D. White, “A universal density profile from hierarchical clustering,” *The Astrophysical Journal*, vol. 490, pp. 493–508, 1997.
- [38] S. Portegies Zwart and S. L. W. McMillan, *Astrophysical Recipes: the art of AMUSE*. AAS IOP Astronomy publishing, 2018.
- [39] S. Portegies Zwart, S. McMillan, A. van Elteren, I. Pelupessy, and N. de Vries, “Multi-physics simulations using a hierarchical interchangeable software interface,” *Computer Physics Communications*, vol. 183, pp. 456–68, 2013.
- [40] F. I. Pelupessy, A. van Elteren, N. de Vries, S. L. W. McMillan, N. Drost, and S. F. Portegies Zwart, “The astrophysical multipurpose software environment,” *Astronomy and Astrophysics*, vol. 557, 2013.

- [41] S. Portegies Zwart, S. McMillan, B. Ó Nualláin, D. Heggie, J. Lombardi, P. Hut, S. Banerjee, H. Belkus, T. Fragos, J. Fregeau, M. Fuji, E. Gaburov, E. Glebbeek, D. Groen, S. Harfst, R. Izzard, M. Jurić, S. Justham, P. Teuben, J. van Bever, O. Yaron, and M. Zemp, “A multiphysics and multiscale software environment for modeling astrophysical systems,” *New Astronomy*, vol. 14, pp. 369–78, 2009.
- [42] S. Chandrasekhar, “Dynamical friction. i. general considerations: the coefficient of dynamical friction,” *Astrophysical Journal*, vol. 97, pp. 255–62, 1943.
- [43] Y. Hashimoto, Y. Funato, and J. Makino, “To circularize or not to circularize?—orbital evolution of satellite galaxies,” *The Astrophysical Journal*, vol. 582, no. 1, pp. 196–201, 2003.
- [44] A. R. Zentner and J. S. Bullock, “Halo substructure and the power spectrum,” *The Astrophysical Journal*, vol. 598, no. 1, pp. 49–74, 2003.
- [45] L. Verlet, “Computer ”experiments” on classical fluids. i. thermodynamical properties of lennard-jones molecules,” *Physical Review*, vol. 159, pp. 98–103, 1967.
- [46] E. Athanassoula, E. Fady, J. C. Lambert, and A. Bosma, “Optimal softening for force calculations in collisionless N-body simulations,” *Monthly Notices of the Royal Astronomical Society*, vol. 314, pp. 475–88, 2000.
- [47] T. Tepper-García, J. Bland-Hawthorn, and D. Li, “The M31/M33 tidal interaction: A hydrodynamic simulation of the extended gas distribution,” *Monthly Notices of the Royal Astronomical Society*, vol. 493, p. 5636–47, 2020.
- [48] M. Fourment and M. R. Gillings, “A comparison of common programming languages used in bioinformatics,” *BMC bioinformatics*, vol. 9, no. 1, p. 82, 2008.
- [49] Z. Malkin, “The current best estimate of the galactocentric distance of the sun based on comparison of different statistical techniques,” *ArXiv e-prints*, 2012.
- [50] J. Godden., “MPhys-Project-N-Body-Code.” <https://github.com/jg572/MPhys-Project-N-Body-Code>, 2020. Last accessed 01 April 2020.
- [51] S. Portegies Zwart, *et al.*, “AMUSE - v13.0.0.” <https://github.com/amusecode/amuse>, 2019. Last accessed 01 April 2020.